Pergamon

Int. J. Heat Mass Transfer. Vol. 37, No. 15, pp. 2221–2230, 1994

0017–9310/94 $7.00+0.00

0017–9310(94)E0059–4

Transport phenomena in non-isothermal flow between co-rotating asymmetrically-heated disks

C. Y. SOONG
Department of Aeronautical Engineering, Chung Cheng Institute of Technology, Tahsi, Taoyuan, Taiwan 33509, Republic of China

and

W. M. YAN
Department of Mechanical Engineering, Hua Fan College of Humanities and Technology, Shihting, Taipei, Taiwan 22305, Republic of China

(*Received* 10 *November* 1993 *and in final form* 28 *January* 1994)

Abstract—The present paper reports a numerical study on laminar mixed convection between two co-rotating asymmetrically-heated disks. The centrifugal-buoyancy effect is considered by invoking the Boussinesq approximation. To investigate the qualitative features of this class of rotation-induced mixed convection, the classical boundary-layer approximation is employed to predict the simultaneous development of flow and temperature fields. Effects of the centrifugal-buoyancy, Coriolis force and asymmetric wall-heating are then examined based on the numerical results. For a typical through-flow Reynolds number in a stable laminar flow regime ($Re = 500$), the threshold, type and location of the flow-reversal at various rotational and wall-heating conditions are studied. Also, the mechanisms of the flow-reversal phenomena are addressed in detail.

INTRODUCTION

FLOW AND HEAT transfer in rotating disk systems are of practical interest due to the relevance to the engineering applications. Thermal–fluid flows in various rotating systems have been studied in the previous work, e.g. rotating-disk contactors [1], gas-turbine and compressor disks [2], and magnetic-disk storage systems [3], etc. As for the rotation-induced buoyancy effect, there have been few studies. For flow between two co-rotating infinite disks, Chew [4] studied the rotation-induced buoyancy effect by using a highly-simplified linear model. Recently, similarity analysis for the mixed convection between infinite coaxial disks was performed to study extensively the influences of centrifugal buoyancy [5]. With a non-isothermal through-flow in wheelspace, mixed convection heat transfer has been studied by invoking boundary-layer approximation [6], and that in a shrouded rotor–stator system was investigated by numerical solution of Navier–Stokes/Boussinesq equations [7]. Centrifugal-buoyancy effects in unsteady flow and heat transfer between coaxial disks have also been investigated [8].

Fluid flows between rotating disks are very complicated in nature due to the possibilities of flow-reversal, unsteadiness and instabilities. For stationary disks, the experimental evidence has shown that the flow may become unstable at through-flow Reynolds number ($Re \equiv u_i s/\nu$) higher than 1200 [9]. The limiting tip Reynolds numbers ($Re_\varphi \equiv \Omega r_0^2/\nu$) for stable laminar flows related to the rotating disk systems are of the order 10^5 [10]. In a recent experimental study on co-rotating disks [11] the results revealed that the limiting condition for stable laminar flow is $Re_\varphi = 2.8 \times 10^5$. In internal flows, usually, the flow-reversal occurs before the presence of the unsteadiness and instability. Therefore, it is worthwhile to study the conditions and mechanisms of flow-reversal phenomena. Due to the change in flow-area in radial direction ($2\pi rs$) and the presence of the centrifugal and Coriolis forces, the mechanisms of flow-reversal in the present rotating flows are more complicated than that in conventional duct flows in gravitational force field. In the latter case the only cause for occurrence of flow-reversal is the buoyancy or, in other words, sufficiently large wall-to-fluid temperature difference (WFTD). However, in the rotating disk systems the flow-reversal may be resulted by the adverse pressure gradient (flow-area expansion) and large WFTD and/or high centrifugal force (large cen-

NOMENCLATURE

C_f	skin friction coefficient, $\mu(\partial u/\partial n)_w/\frac{1}{2}\rho u_i^2$
Gr_Ω	rotational Grashof number, $(\Omega^2 s)\beta\Delta T_c s^3/\nu^2$
h	heat transfer coefficient
j	Colburn heat transfer factor, $2NuPr^{-1/3}/Re^*$
k	thermal conductivity
n	directional normal of the disk walls
Nu	Nusselt number, hs/k
P', p'	dimensionless and dimensional pressure departure, $P' = p'/\rho u_i^2$
Pe	Peclet number, $PrRe$
Pr	Prandtl number, ν/α
q''	heat flux
R, r	dimensionless and dimensional radial coordinate, $R = r/s$
r_q	ratio of wall heat flux at disk 2 to that at disk 1, q''_2/q''_1
r_T	ratio of wall temperature at disk 2 to that at disk 1, $(T_2-T_i)/(T_1-T_i)$
R'	dimensionless relative radial position, $(r-r_i)/s$
Re	through-flow Reynolds number, $u_i s/\nu$
Re^*	alternative form of Reynolds number, $[2\ln(R_o/R_i)/(R_o/R_i-1)]Re$
Re_φ	tip Reynolds number, $\Omega r_o^2/\nu$
Ro	rotation number, $\Omega s/u_i$
s	space between the two disks
T	temperature
ΔT_c	characteristic temperature difference $= (T_1 - T_i)$ for UWT and $(q''_1 s/k)$ for UHF
$\bar{U}, \bar{u}$	dimensionless and dimensional local mean velocity, $\bar{U} = \bar{u}/u_i$
U, V, W	dimensionless velocity components in the radial, tangential and axial directions normalized by u_i
u, v, w	dimensional velocity components in the radial, tangential and axial directions
UHF	uniform heat flux
UWT	uniform wall temperature
Z, z	dimensionless and dimensional axial coordinate, $Z = z/s$.

Greek symbols

α	thermal diffusivity
β	thermal expansion coefficient
θ	dimensionless temperature difference, $(T-T_i)/\Delta T_c$
θ_b	dimensionless bulk temperature, $\int_0^1 U\theta\,dZ/\int_0^1 U\,dZ$
θ_1	dimensionless temperature difference, $(T_1-T_i)/\Delta T_c$
μ	viscosity
ν	kinematic viscosity
ρ	density
Ω	rotational speed.

Subscripts

1	disk 1
2	disk 2
i	inlet
o	outlet
r	reference condition
w	wall condition
Ω	rotational condition.

trifugal-buoyancy). The results in ref. [6] revealed that the buoyancy effects are significant in this class of flows. At $Gr_\Omega = \pm 1000$, for example, the change in skin-friction is about 50% as compared with the buoyancy-free results. Obviously, the buoyancy effect is of influence in the occurrence of flow-reversal, and the effect can be altered by the change in thermal boundary condition. Additionally, near the rotating walls, the pumping effect caused by the Coriolis force can also influence the flow-reversal process. For the difficulties encountered in measurements of local skin-friction, numerical simulation is more appropriate in investigation of flow-reversal phenomena.

In the present work, the co-rotating disk system studied in the previous work [6, 12] is reconsidered, while the emphases are placed on: (1) the thermal effects of asymmetric wall-heating on the transport phenomena; and (2) the combinations of parameters for threshold of flow-reversal. Both thermal boundary conditions of asymmetrically-heated isothermal (UWT) and isoflux (UHF) walls are considered. Boussinesq approximation is invoked to account for the centrifugal-buoyancy effect. In a critical study, Raal [13] has disclosed that the boundary layer (BL) theory is a valid approximation to the non-separated flows (upstream region of flow-reversal location) between the parallel disks. Further, the present authors also showed that the boundary layer solutions were in reasonable agreement with the elliptic solutions for the same flow configuration [6]. In the present study the major interest lies in the non-separated flow region and the occurrence of flow-reversal rather than the reversed flow fields downstream. To avoid the difficulty in determination of downstream conditions and to reduce the computational efforts, the classical boundary-layer approximation is employed to simplify the governing equations. The simultaneously developing mixed convection is then investigated by solving the resultant parabolic system using a marching technique. The present BL solution can provide a better understanding of the qualitative nature of this complicated rotation-induced mixed convection. Effects of both the disk rotation and asymmetric wall-heating on the flow and thermal characteristics as well as the mechanisms of flow-reversal are explored.

ANALYSIS

Problem statement

The rotating disk system at constant rate Ω considered in the present study is schematically shown in Fig. 1. Two parallel heated annular disks with inner and outer radii r_i and r_o are separated by a spacing s. The inlet coolant fluid at a uniform velocity u_i flows radially outward through the flow passage between the disks. The inlet fluid is of uniform temperature T_i, while the disks 1 and 2 are held at uniform temperatures T_1 and T_2 (isothermal walls) or heated by uniform heat fluxes q''_1 and q''_2 (isoflux walls), respectively. A cylindrical polar coordinate (r, z) is fixed on the disk 1 with the origin at the disk center. The fluid flow under consideration is steady, incompressible, axisymmetric, laminar and is of constant properties except the density variation in centrifugal force terms. The boundary-layer approximation is employed to simplify this simultaneously developing flow problem. To consider the buoyancy effect, Boussinesq's approximation is invoked to allow for the density variation, $\rho = \rho_r[1-\beta(T-T_r)]$, in centrifugal force terms. Gravitational effect, in this case, is comparatively small and can be neglected.

Governing equations and boundary conditions

The dimensionless governing equations of boundary-layer form can be written as [6]:

$$\frac{\partial(RU)}{\partial R}+\frac{\partial(RW)}{\partial Z}=0, \qquad (1)$$

$$U\frac{\partial U}{\partial R}-\frac{V^2}{R}+W\frac{\partial U}{\partial Z}=\frac{1}{Re}\frac{\partial^2 U}{\partial Z^2}+2RoV-\frac{Gr_\Omega}{Re}R\theta-\frac{\partial P'}{\partial R}, \qquad (2)$$

$$U\frac{\partial V}{\partial R}+W\frac{\partial V}{\partial Z}+\frac{UV}{R}=\frac{1}{Re}\frac{\partial^2 V}{\partial Z^2}-2RoU, \qquad (3)$$

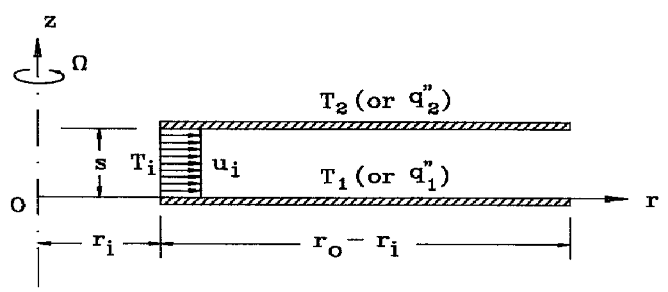

FIG. 1. Flow and heat transfer model of co-rotating disks.

$$U\frac{\partial \theta}{\partial R}+W\frac{\partial \theta}{\partial Z}=\frac{1}{Pe}\frac{\partial^2 \theta}{\partial Z^2}, \qquad (4)$$

and the global continuity is:

$$\int_0^1 RU\,dZ = R_i. \qquad (5)$$

The inlet conditions for this problem are:

$$R = R_i \quad U-1 = V = W = \theta = 0, \qquad (6a)$$

and the wall boundary conditions for disk 1 ($Z = 0$) and disk 2 ($Z = 1$) are:

$$Z=0 \quad U=V=W=0 \quad \text{and} \quad \theta = 1\,(UWT) \quad \text{or} \quad -\partial\theta/\partial Z = 1\,(UHF)$$

$$Z=1 \quad U=V=W=0 \quad \text{and} \quad \theta = r_T\,(UWT) \quad \text{or} \quad \partial\theta/\partial Z = r_q\,(UHF), \qquad (6b)$$

respectively. Where the parameters $r_T = (T_2-T_i)/(T_1-T_i)$ characterizes the ratio of the wall-temperature functions at the two disks, and $r_q = q''_2/q''_1 = (\partial\theta/\partial Z)_2$ is the ratio of the wall heat-flux at disk 2 to that at disk 1.

Governing parameters

In this problem there are two geometry parameters, i.e. the inner and outer radii of the disk system, R_i and R_o. The through-flow Reynolds number Re stands for the forced-flow effects. The effects of Coriolis force and centrifugal-buoyancy are characterized by rotation number Ro and rotational Grashof number Gr_Ω, respectively. The positive values of Gr_Ω correspond to the buoyancy effects retarding the main flow, and the negative ones to that assisting the main flow. The parameters r_T and r_q characterize the asymmetry of wall-heating in isothermal and isoflux cases, respectively. For the cases of symmetric heating, r_T (or r_q) is unity.

In the present study the range of wall-heating parameters is $0 \leqslant r_T$ (or r_q) $\leqslant 1$, the rotation number Ro ranges from 0.02 to 0.08, and the values of $Gr_\Omega = -500$, 0, and 500 are used as the typical values to characterize buoyancy-assisted, buoyancy-free, and buoyancy-opposed flows, respectively. To find the threshold of the flow-reversal, the extended range, $-6000 \leqslant Gr_\Omega \leqslant 2000$, is studied. To reduce the computational efforts, however, the Reynolds number is fixed, $Re = 500$. The details of Reynolds number effects have been reported in the previous study [6].

Flow and heat transfer parameters

Local skin friction coefficient defined as $C_f = \mu(\partial u/\partial n)_w/\frac{1}{2}\rho u_i^2$, where n denotes directional normal of the disk walls ($n = Z$ for disk 1 and $-Z$ for disk 2). Therefore, the skin-friction coefficients for disks 1 and 2 are:

Table 1. Grid-dependence tests on local Nusselt number Nu_1 for the case of $Re = Gr_\Omega = 500$, $Ro = 0.05$, $R_i = 20$, $R_o = 60$ and $r_q = 0.5$

			Nu_1		
R'	401 × 161	201 × 161	201 × 81	201 × 41	101 × 41
1.667	7.712	7.622	7.606	7.510	7.317
6.122	4.740	4.726	4.723	4.703	4.680
12.249	3.850	3.851	3.849	3.841	3.826
20.675	3.528	3.533	3.532	3.526	3.524
32.265	3.385	3.389	3.388	3.383	3.387
40.000	3.301	3.305	3.304	3.300	3.305

$$C_{f1} = \frac{2}{Re}\left[\frac{\partial U}{\partial Z}\right]_{Z=0}$$

and

$$C_{f2} = -\frac{2}{Re}\left[\frac{\partial U}{\partial Z}\right]_{Z=1}. \quad (7)$$

Heat transfer performance is characterized by Nusselt number $Nu = hs/k = -(\partial\theta/\partial n)_w/(\theta_1 - \theta_b)$, where

$$\theta_b = \int_0^1 U\theta \,dZ \Big/ \int_0^1 U \,dZ$$

is dimensionless bulk temperature. The dimensionless expressions for local Nusselt numbers at disk 1 and 2 are:

$$Nu_1 = -\frac{1}{\theta_1 - \theta_b}\left[\frac{\partial\theta}{\partial Z}\right]_{Z=0}$$

and

$$Nu_2 = \frac{1}{\theta_1 - \theta_b}\left[\frac{\partial\theta}{\partial Z}\right]_{Z=1}. \quad (8)$$

NUMERICAL PROCEDURE

The parabolic system, equations (1)–(5) with boundary conditions (6), is solved by using a typical marching technique. Closely packed grids are arranged in entrance and near-wall regions to capture the high gradients of the variables. A numerical experiment is performed to determine the proper grid-arrangement for grid-independent solutions. Nusselt numbers obtained on various grids are listed in Table 1. The deviations of the local heat transfer rates, Nu_1, generated on the grid of $201(R) \times 81(Z)$ from that on the finer grid, i.e. $401(R) \times 161(Z)$, are less than 1.4%. For consideration of reducing computational efforts, the former is adequate and is used through the course of computation. The grid size $\Delta R/(R_o - R_i)$ is varied from the order of 10^{-3} to 10^{-2}. The outer boundary of the computational domain, R_o, in this study is 60. The marching procedure progresses continuously until the pre-set terminal location, $R_o = 60$, is reached or the flow-reversal occurs. The iterative procedure in axial direction is ended as the maximum relative deviations of all dependent variables satisfy the criterion: Max $|(\phi_{i,j}^{new} - \phi_{i,j}^{old})/\phi_{i,j}^{new}| < 10^{-4}$, where ϕ can stand for U, V, or θ. The present solution procedure has been checked by a comparison with the elliptic solutions, and used in the previous studies [8, 9]. Generally speaking, the present BL solutions are reasonable in the parameter ranges considered.

RESULTS AND DISCUSSION

Comparisons with the previous studies

To validate the present numerical solution, the predictions are compared with the previous measured data [14] as well as the Navier–Stokes (N–S) computations [12] for buoyancy-free flows in a co-rotating disk system of $R_o = 103.33$, $R_i = 53.33$ and $r_T = 1.0$. For convenience in comparison, the nomenclature in ref. [15], i.e. the Colburn j-factor, $j = 2NuPr^{-1/3}/Re^*$, and an alternative form of the Reynolds number, $Re^* = [2\ln(R_o/R_i)/(R_o/R_i - 1)]Re$, are used in Fig. 2. It can be observed that the present BL solutions are in good agreement with the computational results of the Navier–Stokes equations for the stationary case. At the rotating rate of $\Omega = 30$ Hz, the rotation number is $Ro = 28.125/Re$ for the present configuration. For small Re, the influence of rotation is relatively important, and the deviation between the BL and the N–S solutions becomes noticeable. However, for the Re-range investigated the agreement between these two solutions is acceptable.

Both the parabolic and elliptic solution procedures under-predict the test results in [14] and the deviation

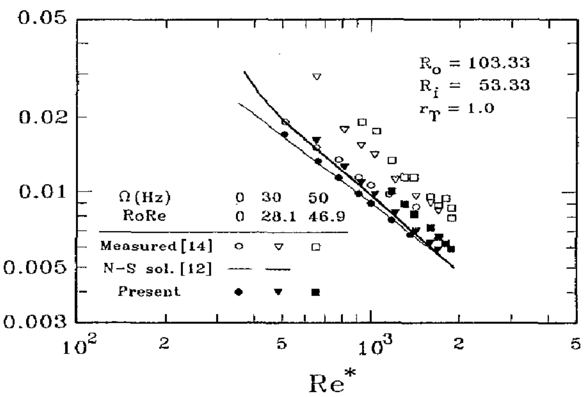

FIG. 2. Comparisons of the present BL solutions with the previous results.

grows as the Reynolds number increases. According to the author's experience in experimental studies on rotating systems [15], the discrepancies between the predictions of the laminar theory and the measurements can be attributed to the uncertain inlet conditions including inlet geometry and initial swirl (or turbulence level) in the test. Besides, in the experiment, the difficulties in heat loss control and the accurate measurement of the temperature/heat flux may also result in uncertainty in the heat transfer rate. Those are also the reasons for the inconsistency of the measured data by various investigators as that mentioned in ref. [16]. In summary, at least for the cases of $RoRe \leqslant 28.125$, the present BL solutions provide almost the same order of accuracy as that of N–S ones, and the predictions also present a reasonable trend as the measured data behave.

Isoflux-disk solutions

Figure 3 shows the radial velocity developments at isoflux condition. In Fig 3a–c the assisting, zero, and opposing buoyancy effects are presented. Since disk 1 ($Z = 0$) is relatively hotter than disk 2 ($Z = 1$) the buoyancy-assisting effect accelerates the fluid near $Z = 0$ for $Gr_\Omega = -500$. Conversely, in Fig. 3c for $Gr_\Omega = 500$ the fluid near the hotter wall, i.e. disk 1, is retarded due to buoyancy-opposing effect. The wall-heating effects can be clearly shown in comparison of Fig. 3d, c and e for different heating rates, $r_q = 0, 0.5$, and 1.0, respectively. In the case with $r_q = 0$ (adiabatic on disk 2) in Fig. 3d, the fluid temperature near $Z = 1$ is nearly the same as the temperature of disk 2, where the buoyancy effect is diminished. While the fluid adjacent to the disk 1 encounters a retarding force due to buoyancy-opposing effect, the velocity distribution is then highly distorted. Figure 3c and f present the Ro-effect on the radial velocities. Obviously, the larger velocity-gradients appear in the case of the larger Coriolis force $Ro = 0.05$.

Figures 4 and 5 show the effects of wall-heating and disk rotation, including centrifugal-buoyancy and Coriolis, on the tangential velocity and temperature developments, respectively. In Fig. 4, it is observed that the thermal effects of buoyancy and wall-heating cause no significant change in tangential velocity distributions, while the Coriolis force does through the action of $-2RoV$. On the other hand, in Fig. 5, the Coriolis effect and centrifugal-buoyancy only slightly alter the temperature fields. However, the changes in flow temperature due to the Coriolis effects seems to be increased along the radial direction. For the cases of $Re = Gr_\Omega = 500$ and $Ro = 0.02$ with the wall-heat-

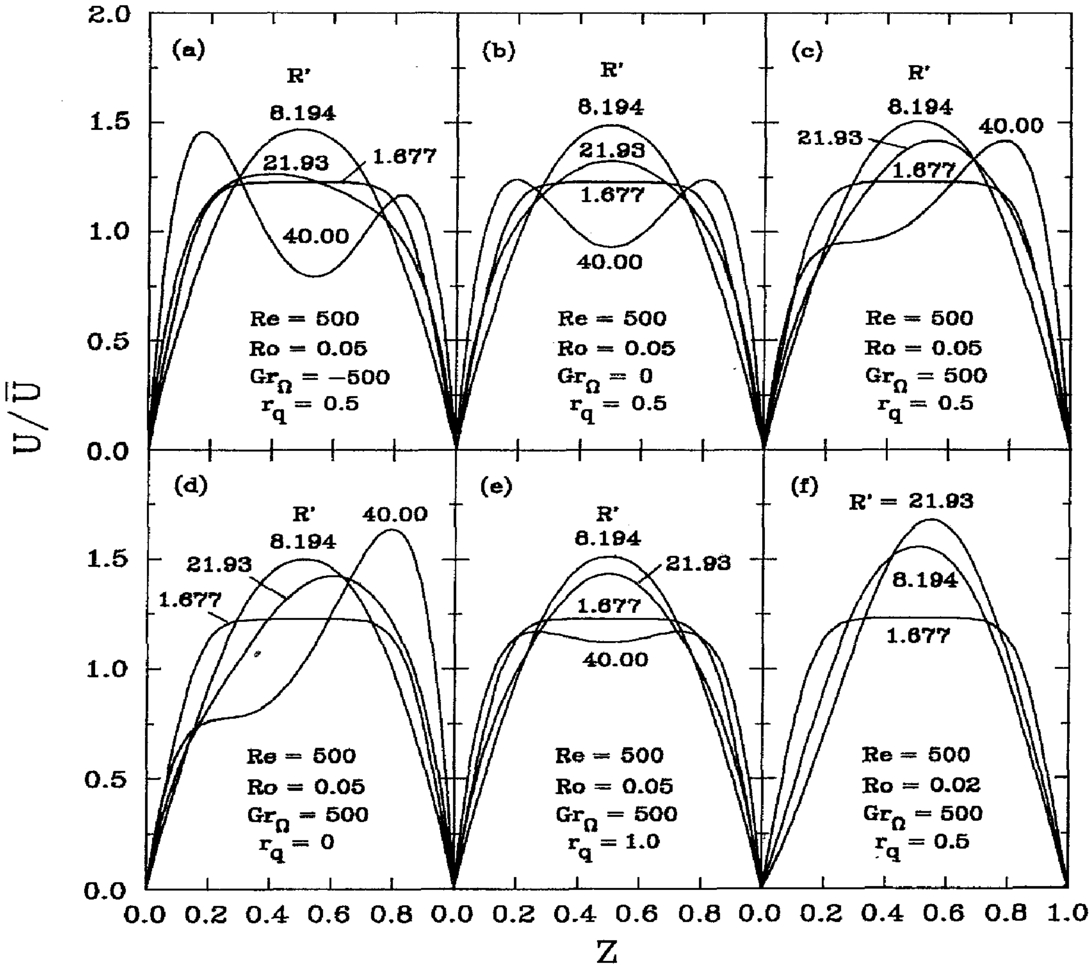

FIG. 3. Axial velocities at various conditions for isoflux disks (UHF), where $R' = R - R_i$.

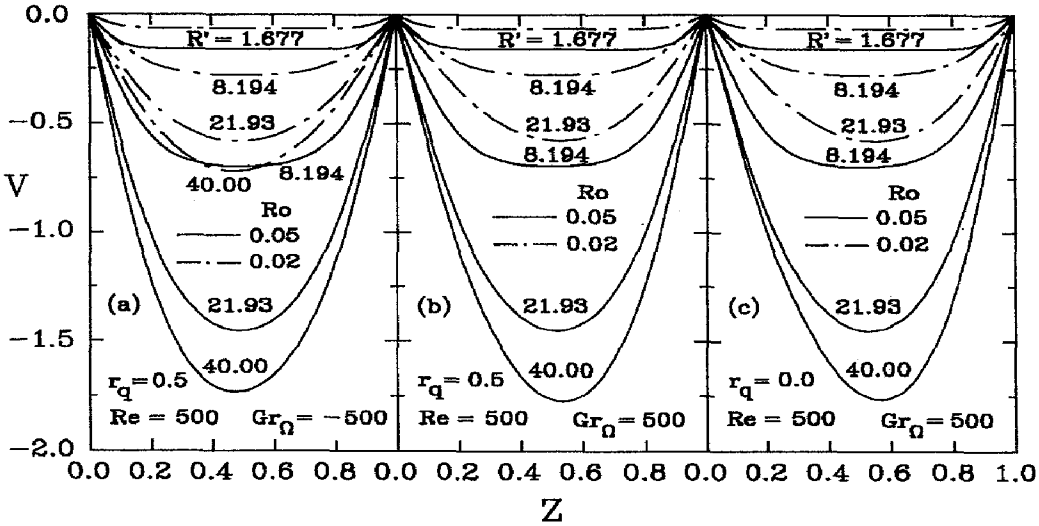

FIG. 4. Tangential velocities for isoflux disks (*UHF*).

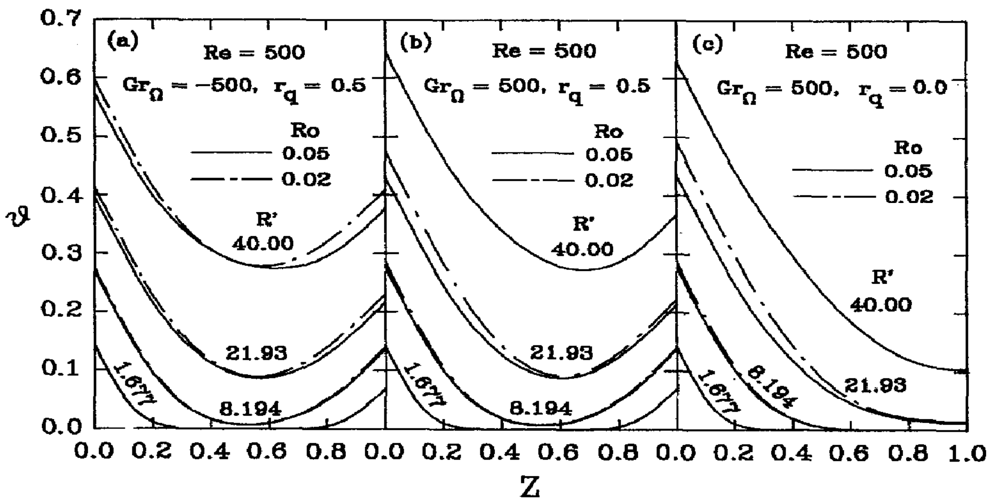

FIG. 5. Temperature fields for isoflux disks (*UHF*).

ing parameters of $r_q = 0$ and 0.5 in Figs. 4 and 5, solutions of V and θ are absent due to the occurrence of flow-reversal phenomena. The flow-reversal in the present flow configuration will be addressed later.

Centrifugal-buoyancy effects on local skin-friction and heat transfer performance are shown in Fig. 6, where $R' = R - R_i$. As disclosed in the previous study [6], the buoyancy-assisting effect enhances the skin friction and heat transfer rates; while the buoyancy-opposing effect alleviates both. Moreover, the results also reveal that the larger buoyancy effects appear on disk 1 rather than on disk 2.

In the case of buoyancy-opposed flow as that of $Re = Gr_\Omega = 500$ and $Ro = 0.05$ shown in Fig. 7, local skin-friction on the disk 2 (C_{f2}) increases as the heating rate r_q is decreased, but the skin friction on the disk 1 (C_{f1}) decreases. This trend can be explained by re-examining Fig. 3e, c and d, where the radial velocity profile becomes asymmetric and gradually leans toward the disk 2 as r_q decreases from 1.0 to 0. Heat transfer rates on disks 1 and 2 decrease with decreasing r_q. The effects of asymmetric wall-heating on skin

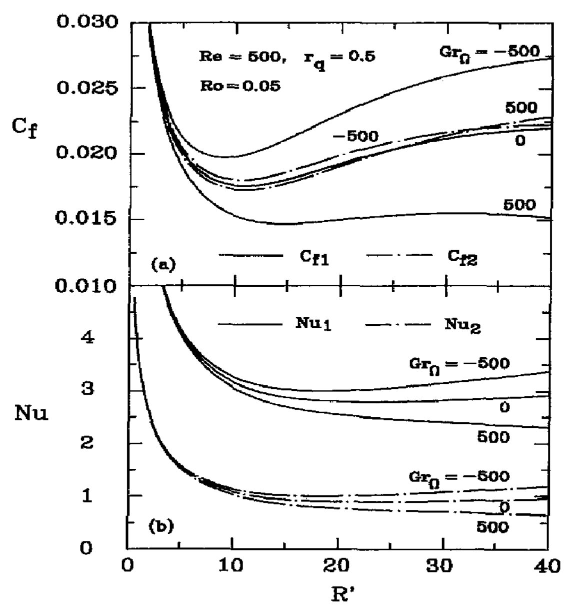

FIG. 6. Centrifugal-buoyancy effects on skin-friction and heat transfer rates (*UHF*).

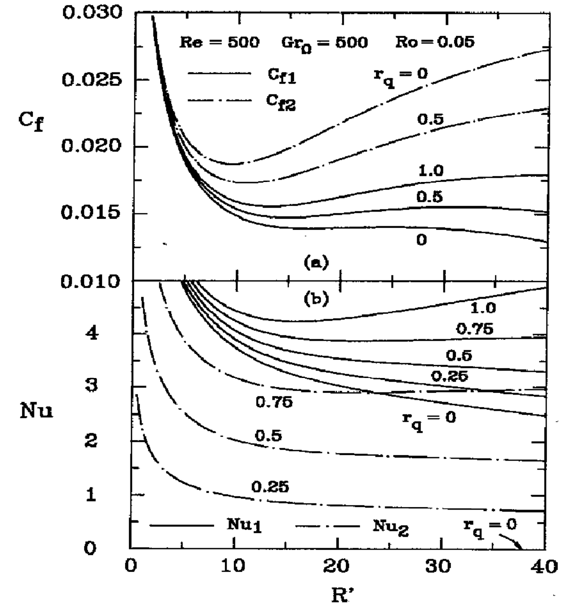

FIG. 7. Wall-heating effects on skin-friction and heat transfer rates (*UHF*).

friction and heat transfer rates become larger at downstream location. It is attributed to the large buoyancy effect resulting from the large centrifugal force.

The Coriolis force can generate pumping effect and, in turn, accelerates the fluid adjacent to the disk walls. Therefore, C_f and Nu both increase with the increasing rotation number Ro. This physical viewpoint can be corroborated by the numerical solutions shown in Fig. 8, in which the pumping effect for the relatively low rotation number, $Ro = 0.02$, is not large enough to resist the retarding effect caused by the centrifugal-buoyancy. The flow-reversal occurs at the disk 1 for the relatively strong buoyancy-opposing effect there. For $Ro = 0.05$ in Fig. 8, the wall-flow reversal is suppressed for the larger Coriolis effect. In the case of $Ro = 0.08$, the velocity solutions and skin-friction near the exit ($R' = 40$) present zigzag behavior. It is believed that, for a high tip Reynolds number ($Re_\varphi = 1.44 \times 10^5$) and the presence of the buoyancy-opposing effect ($Gr_\Omega = 500$) in this case, the flow may become unstable.

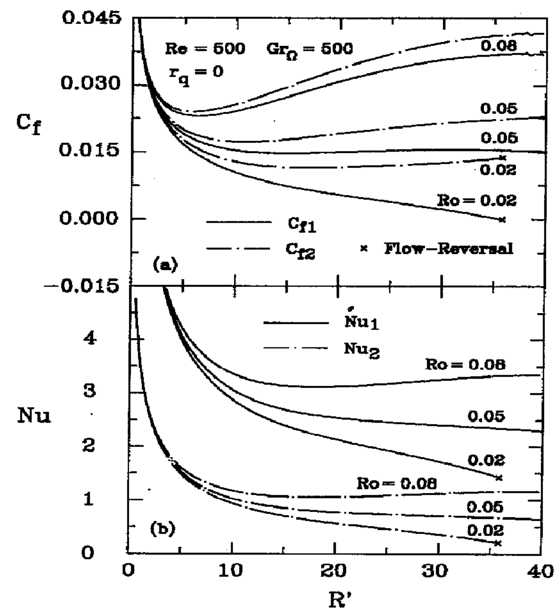

FIG. 8. Coriolis effects on skin-friction and heat transfer rates (*UHF*).

Comparisons of isoflux-disk and isothermal-disk solutions

It has been shown in ref. [6] that the radial velocity distributions for isothermal and isoflux cases have the similar trend, while the temperature fields are somewhat different. In the case of symmetric wall-heating, the WFTD approaches a constant value at *UHF* conditions but diminishes gradually at *UWT* ones [6]. With asymmetric heated walls, however, the WFTD cannot diminish at either *UHF* or *UWT* condition. Figure 9 presents the temperature solutions for isothermal disks at various conditions. Generally speaking, the WFTD noticeably reduces along the radial direction. For the same conditions in Figs 9b and 5b, $Re = Gr_\Omega = 500$ and $r_T = r_q = 0.5$, WFTD for *UWT* is larger than that for *UHF* especially at the upstream locations.

For isothermal cases, the local skin friction and heat transfer rates are plotted in Fig. 10, in which the buoyancy effects dominate in the region near the disk 1. Comparing Figs. 6 and 10 indicates that the local buoyancy effects in isoflux cases increase with R', while in the isothermal ones the changes in C_{f1} and Nu_1 due to the buoyancy effects (parameters associated with the hotter wall) are nearly constant along the radial direction. Note that centrifugal-buoyancy is a coupled effect of the centrifugal force and the temperature non-uniformity. Recall that in the case of *UHF* with $r_q = 0.05$ in Fig. 5b, temperature gradients at the two walls are nearly invariant along the radial direction, especially in the downstream portion of the flow passage. Whereas the centrifugal force increases with the radial position R, therefore, the buoyancy induced by the centrifugal force increases with R' as that shown in Fig. 6b. For the *UWT* case with $r_T = 0.5$ in Fig. 9b, the temperature gradients decrease with flow. In this situation, even though the centrifugal forces increases with R', the centrifugal-buoyancy effects characterized by the difference between Nu-curves for $Gr_\Omega \neq 0$ and $Gr_\Omega = 0$, i.e. $Nu(Gr_\Omega) - Nu(Gr_\Omega = 0)$, are nearly invariant in the downstream portion, $R' > 15$, see Fig. 10b. From the aspect of temperature field developments in Figs. 5 and 9, the effects of asymmetric wall-heating for *UWT* in Fig. 11 are more remarkable than that for *UHF* in Fig. 7.

Flow-reversal phenomena and the mechanisms

For the rotating flow configuration, flow-reversal mechanisms are more complicated than those in conventional channel flows. The following three effects play the important roles in the flow-reversal process.

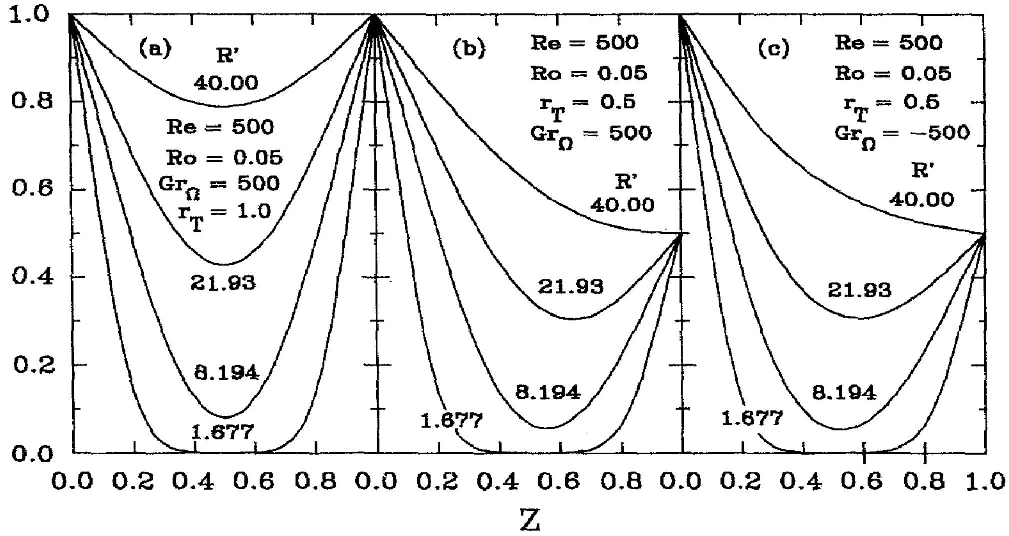

FIG. 9. Temperature solutions at various conditions for isothermal disks (*UWT*).

(1) *Momentum effect*. In the present radial-type flow passage, the pressure first drops near the inlet due to the presence of the strong diffusion, and then increases along the radial direction due to the enlargement of the flow-area. The adverse pressure-gradient in the downstream region may promote or even cause the occurrence of flow-reversal.

(2) *Centrifugal-buoyancy effect*. The buoyancy effect induced by the centrifugal force may distort radial velocity distributions significantly. The fluid in the field is then retarded and, moreover, reversed due to the large centrifugal-buoyancy. The buoyancy may present two kinds of influences in flow fields. One is the so-called buoyancy-assisting effect which accelerates the fluid near the walls, and another is the buoyancy-opposing effect which decelerates the fluid adjacent to the walls. In the situation where the high buoyancy-opposing effect appears, the fluid adjacent to the hot wall may be pushed upstream, and the reversed flow is a wall flow-reversal (WFR) mode. In the buoyancy-assisting case, the fluid near the walls is accelerated and, to satisfy the global continuity, the fluid near the passage center (or off-wall region) has to be decelerated. In the worse case, the fluid somewhere between the walls may be reversed due to the high buoyancy force. The latter is an in-field flow-reversal (IFR) mode.

(3) *Coriolis effect*. For rapidly rotating disks, the radial component of the Coriolis force, $2RoV$, in radial momentum equation generates a strong effect pumping the fluid near the rotating walls radially outwards. Like the near-wall behavior in the buoyancy-assisted flows, this pumping effect will delay the occurrence of WFR and promotes IFR.

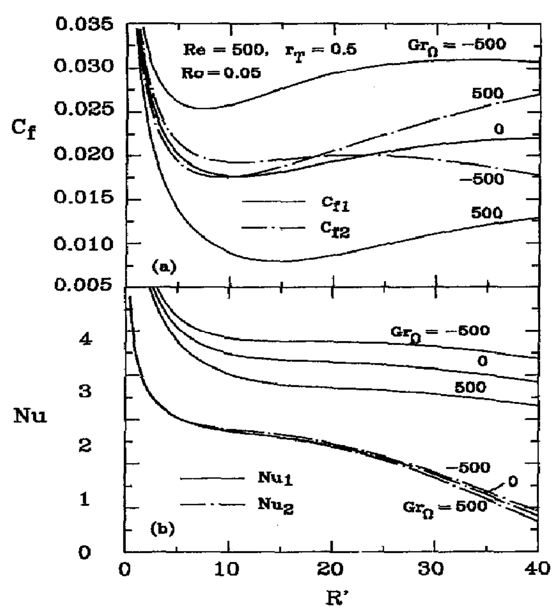

FIG. 10. Centrifugal-buoyancy effects on skin-friction and heat transfer rates (*UWT*).

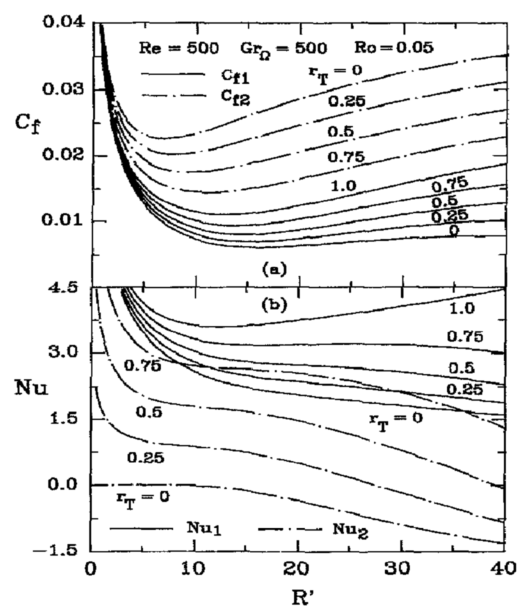

FIG. 11. Wall-heating effects on skin-friction and heat transfer rates (*UWT*).

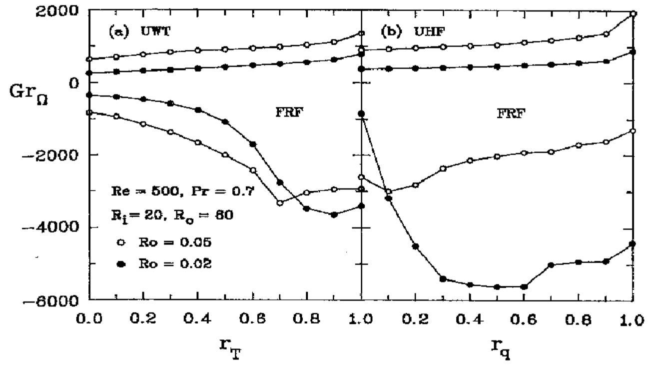

FIG. 12. Parameter-map for threshold of flow-reversal: (a) isothermal disks (*UWT*) and (b) isoflux disks (*UHF*).

Figure 12 shows the parameter-map for flow-reversal phenomena between co-rotating disks, and Table 2 lists the details of the critical conditions for flow-reversal. In Table 2, E stands for the flow-reversal occurring at exit region ($R' > 37.5$) and M for that occurring in mid-way of the radial flow passage, i.e. between the inlet and the exit regions; while W and I denote WFR and IFR modes, respectively. For both *UWT* and *UHF*, it is observed that the WFR mode is prevalent for the cases for $Gr_\Omega > 0$. In this situation, the Coriolis effect can delay the flow-reversal and enlarge the flow-reversal-free (FRF) region in Fig. 12. In the buoyancy-assisted flow ($Gr_\Omega < 0$), the influences of Coriolis force depend on the flow-reversal mode. At the conditions of *UWT* and $Gr_\Omega < 0$, for instance, the strong Coriolis effect ($Ro = 0.05$) delays WFR at $r_T \leqslant 0.7$ and promotes IFR at $r_T > 0.7$. The same argument is also available for interpretation of the flow-reversal map for *UHF*, where the flow-reversal mode switches at r_q between 0.1 and 0.2. The wall-heating effect is an important parameter for the threshold of flow-reversal. The present results reveal that the asymmetry of wall-heating simply promotes the occurrence of flow-reversal for $Gr_\Omega > 0$ under either *UWT* or *UHF* condition. For $Gr_\Omega < 0$, as shown in Table 2, the IFR mode occurs in most cases, especially for the higher rotation number, $Ro = 0.05$. Due to rather complicated nature of velocity distortion in IFR mode, the effect of asymmetric wall-heating on the threshold of flow-reversal cannot follow a simple rule as that mentioned for $Gr_\Omega > 0$.

CONCLUDING REMARKS

The present study has performed a numerical investigation for simultaneously developing laminar mixed convection between two asymmetrically-heated co-rotating disks. Based on the present results, the following conclusions about the qualitative features of this flow configuration can be drawn.

(1) Rotational effects, including Coriolis and centrifugal-buoyancy, are both significant in this class of rotating flows. For either *UHF* or *UWT* condition, the Coriolis force can enhance both skin-friction and heat transfer rates. However, the effects of the centrifugal-buoyancy are rather

Table 2. Flow-reversal in mixed convection between co-rotating disks at $Re = 500$, $Pr = 0.7$, $R_i = 20$, $R_o = 60$, grid $= 201 \times 81$

	$Ro = 0.05$		$Ro = 0.02$	
r†	$Gr_\Omega > 0$	$Gr_\Omega < 0$	$Gr_\Omega > 0$	$Gr_\Omega < 0$
(A) Isothermal walls (*UWT*):				
0.0	638 (E, W)	−824 (E, I)	255 (E, W)	−350 (E, W)
0.1	693 (E, W)	−949 (E, I)	275 (E, W)	−406 (E, W)
0.2	756 (E, W)	−1164 (E, I)	299 (E, W)	−483 (E, W)
0.3	825 (E, W)	−1390 (E, I)	327 (E, W)	−596 (E, W)
0.4	876 (M, W)	−1677 (E, I)	361 (E, W)	−774 (E, W)
0.5	904 (M, W)	−2015 (E, I)	404 (E, W)	−1091 (E, W)
0.6	936 (M, W)	−2430 (E, I)	456 (M, W)	−1724 (E, W)
0.7	978 (M, W)	−3340 (E, I)	499 (M, W)	−2764 (E, W)
0.8	1034 (M, W)	−3050 (M, I)	553 (M, W)	−3483 (M, I)
0.9	1119 (M, W)	−2950 (M, I)	628 (M, W)	−3649 (M, I)
1.0	1354 (M, W)	−2930 (M, I)	784 (M, W)	−3410 (M, I)
(B) Isoflux walls (*UHF*)				
0.0	903 (E, W)	−2606 (E, I)	362 (E, W)	−850 (M, W)
0.1	924 (E, W)	−3005 (E, I)	376 (E, W)	−3196 (E, W)
0.2	964 (E, W)	−2816 (E, I)	390 (E, W)	−4501 (E, I)
0.3	996 (E, W)	−2360 (E, I)	406 (E, W)	−5404 (E, I)
0.4	1026 (E, W)	−2142 (E, I)	426 (E, W)	−5558 (E, I)
0.5	1048 (E, W)	−2028 (E, I)	448 (E, W)	−5624 (E, I)
0.6	1123 (E, W)	−1922 (E, I)	474 (E, W)	−5612 (E, I)
0.7	1183 (E, W)	−1886 (E, I)	506 (E, W)	−5012 (E, I)
0.8	1262 (E, W)	−1704 (E, I)	550 (E, W)	−4922 (E, I)
0.9	1376 (E, W)	−1610 (E, I)	616 (E, W)	−4906 (E, I)
1.0	1945 (E, W)	−1300 (E, I)	888 (E, W)	−4410 (E, I)

Note: E = exit, M = mid-way, I = IFR mode, W = WFR mode.
† For *UWT* $r = r_T$; for *UHF* $r = r_q$.

complicated due to the dependence of the magnitude of the centrifugal force as well as the wall-heating conditions. In the cases studied, the noticeable buoyancy effects on the hotter wall (disk 1) are observed and the effects on the cooler one (disk 2) are small.

(2) In a comparison of the two kinds of thermal boundary conditions, the centrifugal-buoyancy effects on C_{f1} and Nu_1 increase along the radial direction for the isoflux disks; while, in the case of isothermal disks, the buoyancy effects on the local values of C_{f1} and Nu_1 cease to grow for $R' > 15$. This is attributed to the distinct radial evolutions of fluid temperature and, therefore, WFTD under the two different thermal boundary conditions.

(3) Increasing the degree of the wall-heating asymmetry, i.e. decreasing r_q or r_T, degenerates the heat transfer performance of the two walls and also alleviates the friction factor of the cooler wall, C_{f2}, but enhances the friction factor of the disk 1, C_{f1}. Generally speaking, with the same value of r_q and r_T, the effects of the asymmetric wall-heating for *UWT* appear larger than those for *UHF*.

(4) The critical values of Gr_Ω for flow-reversal can be significantly influenced by the Coriolis effect as well as the thermal boundary conditions. In general, the flow-reversal of WFR mode can be delayed by the near-wall pumping effect of the Coriolis force. Conversely, the IFR mode is promoted by the Coriolis effect. The asymmetric wall-heating may cause premature flow-reversal in buoyancy-opposed flows ($Gr_\Omega > 0$) for either *UWT* or *UHF* cases. For buoyancy-assisted flows ($Gr_\Omega < 0$), however, there is the anomalous behavior of the critical Gr_Ω due to the complicated coupling of the hydrodynamic and thermal effects.

(5) At various rotational and thermal conditions, the flow-reversal-free region for $Gr_\Omega < 0$ is larger than that for $Gr_\Omega > 0$. In other words, the occurrence of flow-reversal is easier in buoyancy-opposed flows. Therefore, it can be expected that the buoyancy-assisted flows are more stable than the buoyancy-opposed ones. To corroborate this point, a stability analysis is very appropriate.

Acknowledgement—The financial support of this research by the National Science Council of the Republic of China through Grant NSC-82-0401-E-211-502 is greatly appreciated.

REFERENCES

1. W. J. Yang, Gas–liquid mass transfer in rotating performance disc contactors, *Lett. Heat Mass Transfer* **9**, 119–129 (1982).
2. J. M. Owen, Fluid flow and heat transfer in rotating disc systems, Int. Centre for Heat Transfer Series. In *Heat and Mass Transfer in Rotating Machinery* (Edited by D. E. Metzger and N. H. Afgan), pp. 81–103. Hemisphere, Washington, DC (1984).
3. C. J. Chang, C. A. Schuler, J. A. C. Humphrey and R. Greif, Flow and heat transfer in the space between two corotating disks in an axisymmetric enclosure, *ASME J. Heat Transfer* **111**, 625–632 (1989).
4. J. W. Chew, Similarity solutions for non-isothermal flow between infinite rotating disks, Report No. TFMRC/38, Thermo-Fluid Mech. Res. Centre, School Eng. Appl. Sci., Univ. Sussex (August 1981).
5. C. Y. Soong, Axisymmetric mixed convection between rotating coaxial disks, submitted to *Int. J. Heat Mass Transfer*.
6. C. Y. Soong and W. M. Yan, Numerical study of mixed convection between two symmetrically heated co-rotating disks, *AIAA J. Thermophys. Heat Transfer* **7**, 165–171 (1992).
7. C. Y. Soong and R. T. Tzong, Numerical investigation of flow and heat transfer in a shrouded rotor–statorsystem, *Proceedings of the* 33*rd Aeronautics and Astronautics Conference*, AASRC, Taipei, Taiwan, ROC, pp. 831–842 (Dec. 1991).
8. C. Y. Soong, Numerical study of fluctuating mixed convection between rotating coaxial disks. In *Numerical Methods in Laminar and Turbulent Flow*, Vol. VIII (Edited by C. Taylor *et al.*), pp. 436–444. Pineridge, Swansea (1993).
9. S. Mochizuki and W. J. Yang, Local heat transfer performance and mechanisms in radial flow between parallel disks, *AIAA J. Thermophys. Heat Transfer* **1**, 112–116 (1987).
10. J. M. Owen and R. H. Rogers, *Flow and Heat Transfer in Rotating-Disc Systems*, Vol. 1: *Rotor–Stator Systems*. John Wiley, New York (1989).
11. S. Mochizuki and T. Inoue, Self-sustained flow oscillations and heat transfer in radial flow through co-rotating parallel disks, *Exper. Thermal Fluid Sci.* **3**, 242–248 (1990).
12. Y. S. Sim and W. J. Yang, Numerical study on heat transfer in laminar flow through co-rotating parallel disks, *Int. J. Heat Mass Transfer* **27**, 1963–1970 (1984).
13. J. D. Raal, Radial source flow between parallel disks, *J. Fluid Mech.* **85**, 401–416 (1978).
14. S. Mochizuki and W. J. Yang, Heat transfer and friction loss in laminar radial flows through rotation annular disks, *ASME J. Heat Transfer* **103**, 212–217 (1981).
15. C. Y. Soong, S. T. Lin and G. J. Hwang, An experimental study of convective heat transfer in radially rotating rectangular ducts, *ASME J. Heat Transfer* **113**, 604–611 (1991).
16. N. V. Suryanarayana, T. Scofield and R. E. Kleiss, Heat transfer to a fluid in radial, outward flow between two coaxial stationary or corotating disks, *ASME J. Heat Transfer* **105**, 519–526 (1983).